Journal of Alloys and Compounds 505 (2010) 188–193

Contents lists available at ScienceDirect

Journal of Alloys and Compounds

journal homepage: www.elsevier.com/locate/jallcom

Effects of fluoride on the structure and properties of microarc oxidation coating on aluminium alloy

Zhijiang Wang[a,b], Lina Wu[a], Wei Cai[b], Shan A[c], Zhaohua Jiang[a,*]

[a] School of Chemical Engineering and Technology, Harbin Institute of Technology, Harbin 150001, PR China
[b] School of Materials Science and Engineering, Harbin Institute of Technology, Harbin 150001, PR China
[c] Chemical Engineering College, Inner Mongolia University of Technology, Hohhot 010051, PR China

ARTICLE INFO

Article history:
Received 6 July 2009
Received in revised form 2 June 2010
Accepted 10 June 2010
Available online 16 June 2010

Keywords:
Microarc oxidation
Aluminium alloy
Fluoride
Corrosion resistance
Tribological properties

ABSTRACT

The composition of electrolyte plays a key role in the structure and properties of the synthesized ceramic coating by microarc oxidation (MAO) process. In the present study, F^- ion, the smallest size among the negative ions, is chosen as the additive. The effects of F^- ion on the structure and properties of the formed ceramic coating have been investigated in detail. Inspection of the scanning electron microscopy (SEM) and X-ray diffraction (XRD) suggests that the addition of fluoride during MAO process can decrease the porosity of the surface and enhance the density of the coating. These structure features lead to the corrosion resistances and tribological properties greatly improved. Based on the experimental results and the characteristics of MAO process, the influence mechanism of F^- is proposed.

1. Introduction

Aluminium and its alloys are of great importance in engineering due to their excellent properties, such as high specific strength, light mass. However, poor surface hardness and corrosion resistance properties have seriously restricted their extensive applications in various industry sectors [1–3]. There is an increasing need to widely broaden the applications range of aluminium alloys through appropriate surface engineering. Hard anodizing is a traditional route to improve the load-bearing capacity of aluminium alloys; however, the hardness and thickness of the oxide layer are often incompetent to endure rigid working conditions [4]. Microarc oxidation (MAO), also called 'micro-plasma oxidation', 'anode spark electrolysis', 'plasma electrolytic anode treatment' and 'plasma electrolytic oxidation', as a rapid and effective means to provide modified surfaces, is gaining increased attention [5–11]. It is a technique that operates at potentials above the breakdown voltage of an oxide film growing on the surface of a passivated metal anode and is characterized by multiple arcs moving rapidly over the treated surface. A plasma environment is generated and a ceramic coating can thus be formed on the metal surface through plasma chemical interactions. The coatings obtained by MAO possess excellent wear resistance and high adhesion to the substrate [12–17]. Therefore, MAO technique has been widely used to produce ceramic coatings on aluminium alloy. Various programs have been undertaken to promote its industrial applications, such as aerospace, automotive, vessels, medicine, textile engineering, and chemical industry.

The composition of electrolyte plays a key role in the structure and properties of ceramic coating formed by MAO [6,18,19]. Wang et al. [20] and Zheng et al. [21] have found that Na_2WO_4 could improve the formation of Al_2O_3 phase in the ceramic coating and improve its wear resistance. Butyagin et al. [22] reveal that introducing compounds of transition metals into the solution can lead to the changes in the coatings' structure, and the coatings obtained are capable of enduring higher thermocyclic loads.

Curran and Clyne [10] confirm that the ceramic coating formed by MAO contains a fairly dense network of shrinkage pipes in the inner compact layer and some channels appeared to penetrate the entire coating. As is well known, F^- is the minimum ion in size among all negative ions, which may enter into the micropipes and further change the structure and properties of the generated coating. Herein, we chose NaF as the additive and studied its effects on the structure and properties of the yielded ceramic coating on the Al alloy substrate by MAO process. It is found that NaF can evidently change the structure and phase composition of the ceramic coating. As well, the corrosion resistance, mechanical and tribological

* Corresponding author. Tel.: +86 451 86402805; fax: +86 451 86402805.
E-mail address: jiangzhaohua@hit.edu.cn (Z. Jiang).

0925-8388/$ – see front matter © 2010 Elsevier B.V. All rights reserved.
doi:10.1016/j.jallcom.2010.06.027

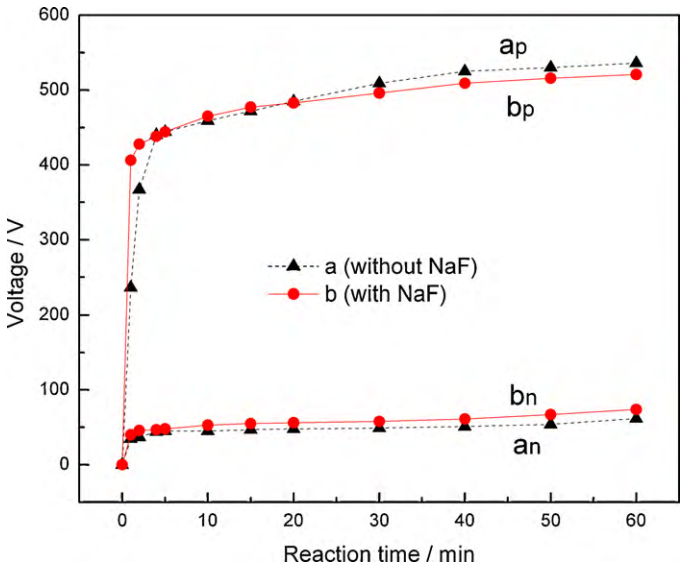

Fig. 1. Voltage–time response of the MAO process in solutions (a_p, a_n-positive and negative voltages in solution without NaF, b_p, b_n-positive and negative voltages in solution with NaF).

properties are optimized. Based on the experimental results and the characteristics of the MAO process, the influence mechanism of F^- is proposed.

2. Experimental

2.1. Preparation of MAO coating

An LY12 Aluminium alloy, having the nominal composition in weight percentage: 3.8–4.9% Cu, 1.2–1.8% Mg, 0.3–0.9% Mn, 0.50% Fe, 0.50% Si, 0.30% Zn, 0.10% Ni, and 0.15% Ti (all values being in wt%), was used as the substrate in the present study. The samples of reaction rectangular dimension of 30 mm × 15 mm × 1 mm were polished with abrasive paper. A homemade pulsed bi-polar electric source of 4 kW was used for the MAO process. One output of the power supply was connected to the container that was made of stainless steel, and the other was connected to the sample immersed in the electrolyte. The ratio of cathodic (I_c) to anodic (I_a) current was set as 1. The constant current density was kept at 8 A/dm^2 under the frequency of 50 Hz and maintained by modulating the voltage. The temperature of electrolyte was kept below 35 °C by adjusting cooling water flow during the MAO process. The electrolytic solutions were composed of 8 g/L $NaAlO_2$ with or without 2 g/L NaF. All the samples were treated in the electrolytic solutions for 60 min. After the treatment, the coated samples were rinsed with distilled water and dried in the air.

2.2. Characterization of MAO coating

The phase composition of the coatings was examined with a RICOH D/max-rB automatic XRD using a CuKα source. The morphology of the coatings was studied by SEM (Hitachi S-4700, Tokyo, Japan).

The accelerated electrochemical measures were evaluated in a three-electrode experimental corrosion cell (a Pt plate as a counter electrode, a saturated calomel electrode as the reference electrode, and 1 cm^2 of the coated sample as the working electrode). A CHI 640B electrochemical analyzer (Shanghai, China) was used to assess the corrosion resistance of the coated samples in aerated 3.5 wt% NaCl solution open to air. General corrosion resistance of the coating was evaluated by polarization curves. The polarization curve scanning rate was 1 mV/s. The polarization corrosion voltage swept from 250 mV below to 250 mV above the open circuit potential. Pitting corrosion resistance was evaluated by potentiodynamic anodic scanning curves. The potentiodynamic scanning rate was 5 mV/s. The potential increased from −0.6 V to −0.4 V, and returned to −0.6 V to form a potential–current density curve. Three parallel samples were used in each measurement of the corrosion resistance to ensure the reliability of experiment results.

The hardness of samples was evaluated using a HVS-1000 Hardness tester with Knoop indenter on the surface of the samples, at a load of 50 g and for a loading duration of 10 s. The final hardness value was the average of 10 replicate measurements.

The tribological behaviors of the samples were evaluated using a ball-on-disc tester (SRVII Friction-Wear Tester) under the dry sliding conditions. GCr15 ball with a diameter of 15 mm and a surface roughness better than 0.05 μm was used as the counterface materials. The measurement of friction coefficient was performed at the load of 2 N and the sliding speed of 150 rpm. A computer was connected to the tester recording the friction coefficient curves. The wear property of the coatings was evaluated by the weight loss of worn samples which were worn under a high load of 80 N. After a selected number of revolutions the weight loss of the samples is determined by an analytical balance with a resolution of 0.01 mg. All the tests were run in the laboratory air (25 °C and relative humidity of 50%). Five parallel samples were used in each tribological test to ensure the reliability of the experiment results.

3. Results

3.1. Voltage–time response

Fig. 1 shows the variation of the cell voltage with treatment time in solutions (one containing 8 g/L $NaAlO_2$, the other containing 8 g/L $NaAlO_2$ and 2 g/L NaF) at a constant applied current density of 8 A/dm^2. It can be seen that the MAO process is simply divided into two stages: a rapidly rising stage where the voltage increased sharply and a relatively stable stage where sparks found on the anode surface and the voltage varying with time at a low ratio. In the range of positive voltage, compared to the electrolyte solution without NaF, the cell voltage increases in a higher rate at the first stage when the electrolyte solution containing NaF. When spark discharge floating on the surface of the sample, the cell voltage increases in lower speed in the solution with NaF. Ranging from the time of 20 min to the process end, the solution without NaF always keeps a higher cell voltage than the solution with NaF. In the range of negative voltage, the solution with NaF always has higher cell voltage than the solution without NaF during the MAO process.

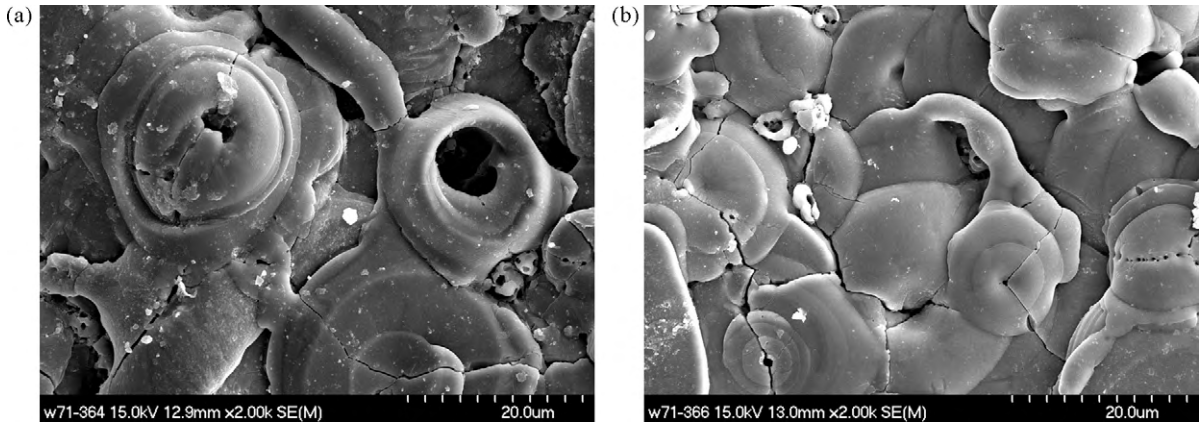

Fig. 2. SEM micrographs of the surfaces of the ceramic coatings: (a) formed in solution without NaF; (b) formed in solution with NaF.

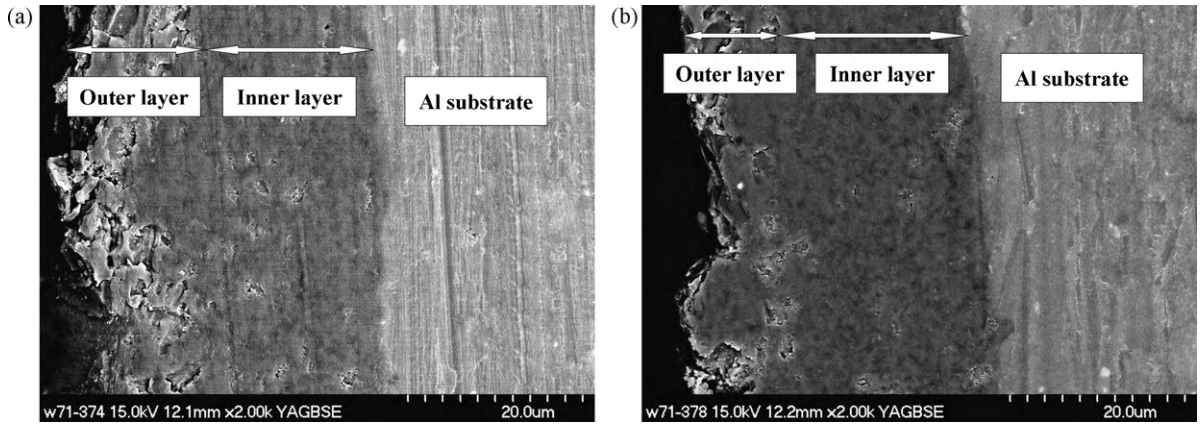

Fig. 3. SEM micrographs of the cross-section of the ceramic coatings: (a) formed in solution without NaF; (b) formed in solution with NaF.

3.2. Structure and morphology of the coatings

Fig. 2 illustrates the surface features of the MAO coating formed in solution without and with NaF. It displays the typical surface morphology of ceramic coating prepared by MAO process, which is caused by the molten alumina flowed out of the discharge channel and rapidly solidified due to the quenching effect by the surrounding electrolyte. There are cracks on the coating surface, which formed due to the internal stresses caused by the constant effect of plasma discharges on the coating. The surface of the sample prepared in solution without NaF is made of island-like structure which has the features of porosity and roughness. There are discharge channels left on the surface, and the diameter of the biggest one is about 8 μm. The surface morphology of the sample formed in the solution with NaF hold the characteristic of lower roughness and porosity. The pancake-like structure is formed on the surface.

The microstructures of the cross-section of the coatings are presented in Fig. 3. Cross-sections of the coating appear as a ceramic structure formed in consequence of multiple local melting by electric discharges and instantaneous quenching by the electrolyte. Both cross-sections show similar thickness and two layers: a porous outer layer and a compact inner layer. There are micropipes and microcracks in the outer layer of the coating. As far as the coating formed in solution without NaF is concerned, the thickness of the porous layer and the compact layer is 15.6 μm and 17.0 μm, respectively. Correspondingly, the thickness of the porous layer and the compact layer of the coating formed with NaF is 11.5 μm and 21.3 μm, respectively. It is clear that coating prepared in solution with NaF possesses a more compact structure.

Fig. 4 is X-ray diffraction patterns of the samples. The results indicate that the MAO coating is composed of α-Al_2O_3 and γ-Al_2O_3. The alumina is produced by plasma thermal chemical reactions in the discharging channels. That there appears an amount of aluminium in the pattern is due to X-ray penetration through to the aluminium substrate [10]. With the addition of NaF into the aluminate solution, we can find that the XRD peak intensity of α-Al_2O_3 and γ-Al_2O_3 increase while the XRD peak intensity of Aluminium decreases. It can be inferred that the X-ray penetrating depth in the coating formed without NaF is larger than that formed with NaF.

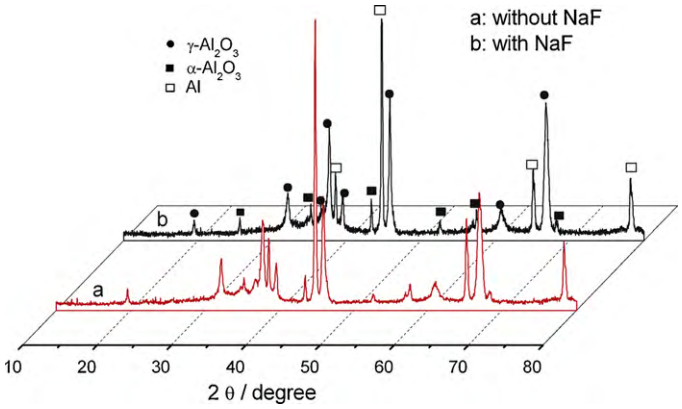

Fig. 4. X-ray diffraction spectra of the ceramic coatings formed in solution with and without NaF.

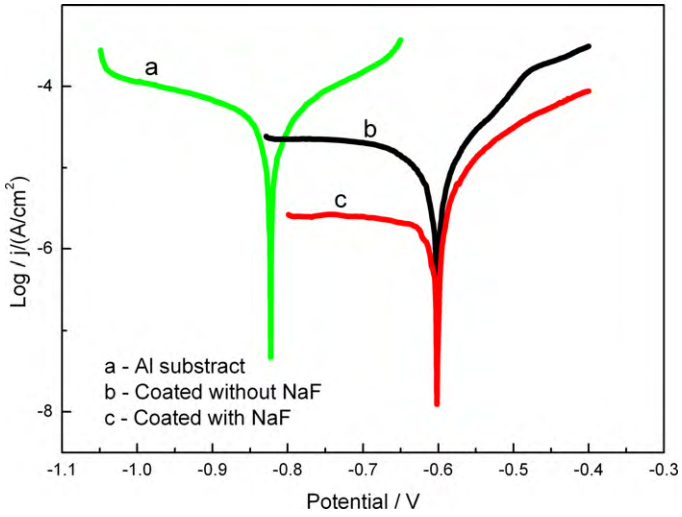

Fig. 5. Polarizing curves of the ceramic coatings formed in solution with and without NaF as well as Al substrate in an aerated 3.5 wt% NaCl solution.

Table 1
The results of potentiodynamic corrosion tests of the samples.

	Al substrate	Coated without NaF	Coated with NaF
E_{corr} (V)	−0.823	−0.601	−0.602
$j_{corr} \times 10^{-7}$ (A/cm^2)	8.86	1.85	0.88
Anodic Tafel slope (β_A), $\times 10^2$ mV/decade	4.90	8.56	5.68
Cathode Tafel slope (β_C), $\times 10^2$ mV/decade	2.44	1.25	6.95
R_p, $\times 10^7$ Ω/cm^2	0.08	0.26	1.54

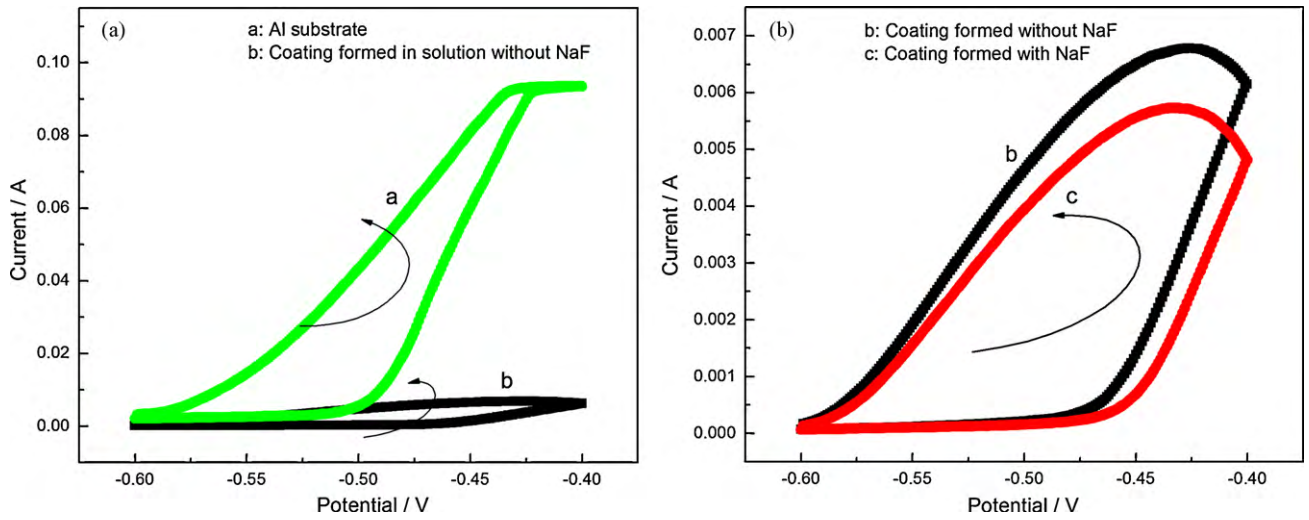

Fig. 6. Potentiodynamic anodic curves of the ceramic coatings formed in solution with and without NaF as well as Al substrate in an aerated 3.5 wt% NaCl solution.

This comparison further confirms that the ceramic coating formed with NaF is more compact than that formed without NaF.

SEM and XRD results reveal several important features of the ceramic coating prepared in solution with NaF. Firstly, there is lower porosity left on the surface of the coating. Secondly, the coating holds a less rough surface. Thirdly, the layer structure of the coating is changed, and the formed coating possesses more compact structure.

3.3. Corrosion resistances of the coatings

3.3.1. General corrosion resistance of the coatings

The polarization behavior of the ceramic coated samples and aluminium substrate are presented in Fig. 5. The corrosion potentials, corrosion rates and anodic/cathodic Tafel slopes (β_A and β_C) were calculated from these tests. Based on the approximate linear polarization at the corrosion potential (E_{corr}), polarization resistance (R_p) values were determined by the following relationship [23]:

$$R_p = \frac{\beta_A \cdot \beta_C}{2.3 j_{corr}(\beta_A + \beta_C)} \quad (1)$$

where j_{corr} is the corrosion current density. A summary of the electrochemical corrosion parameters derived from the potentiodynamic polarization curves are given in Table 1.

Apparently, the ceramic coated samples possess much higher corrosion potential and polarization resistance than uncoated Al alloy. The MAO processed samples exhibit excellent general corrosion resistance. With addition of NaF into the solution, the corrosion potential keeps little change, but the polarization resistance increases from $0.26 \times 10^7\ \Omega/cm^2$ to $1.54 \times 10^7\ \Omega/cm^2$. This result indicates that the general corrosion resistance of the coatings is pronounced improved in the presence of NaF.

3.3.2. Pitting corrosion resistance of the coatings

Fig. 6 shows the potentiodynamic anodic scanning curves of the ceramic coated samples and aluminium substrate. The suddenly rapid potential during the positive scanning is named as broken potential (E_b), which is also called the pitting corrosion potential. The pitting corrosion is determined by E_b. The larger the E_b possesses, the more difficult pitting corrosion occurs. The potentiodynamic loop area reflects the extent of the pitting corrosion development after it occurs. The smaller the loop area, the better the pitting resistance of the corresponding samples [19,24]. The broken potential (E_b) and the area of closed curves of the ceramic coated samples and Al substrate in an aerated 3.5 wt% NaCl solution are presented in Table 2. It can be noted that the pitting corrosion potentials of the ceramic coated samples are all much higher than that of aluminium substrate, which means that the MAO treatment can notably improve the pitting corrosion resistance of Al alloy. The broken potential E_b of the coating prepared without and with NaF is −0.48 V and −0.46 V, respectively. The area of closed curves of the coating prepared in solution without and with NaF is 0.60×10^{-3} and 0.53×10^{-3}, respectively. The coating formed with NaF possesses a higher E_b and a smaller loop area, which demonstrates that this coating has a better localized pitting corrosion resistance.

Table 2
Potentiodynamic anodic scanning results of the samples.

	Al substrate	Coated without NaF	Coated with NaF
E_b (V)	−0.51	−0.48	−0.46
Area, $\times 10^{-3}$ V A	3.47	0.60	0.53

3.4. Mechanical and tribological properties of the coatings

3.4.1. Hardness of the coatings

Fig. 7 shows the hardness of the MAO coatings prepared from the electrolytic solutions without and with NaF. The hardness of the Al alloy substrate is also presented for comparison. It is evident that the hardness of the MAO coatings is much higher than that of the aluminium alloy, which is owing to the formation of α-Al_2O_3 and γ-Al_2O_3 on the substrate of aluminium alloy substrate. When NaF was added into the solution, the prepared ceramic coating has a higher hardness, and the average hardness changes from 1210 HV to 1630 HV.

3.4.2. Wear resistance of the coatings

Fig. 8 demonstrates the weight loss of the samples worn against GCr15 steel ball as a function of the revolution numbers. At the beginning, the weight of the coatings is sharply reduced, and then the weight loss ratio varying with the number of revolutions is lower. This is ascribed to the porous top layer of the coatings worn off at the beginning. Once the dense intermediate layer is revealed, the wear rate of the alumina coatings falls greatly. The weight loss of the coating formed without NaF is always more than that of the coating formed with NaF at the same time. The less weight loss, the better wear resistance. Obviously, compared to the coating formed

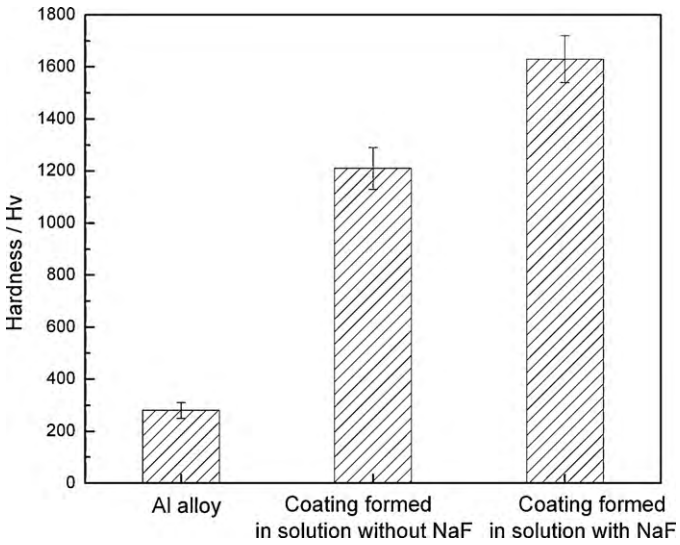

Fig. 7. Hardness of ceramic coatings and Al alloy substrate.

without NaF, the coating formed with NaF possesses a better wear resistance.

3.4.3. *Friction coefficients of the coatings*

Fig. 9 shows the evolution of the friction coefficients versus sliding distance for the ceramic coatings against GCr15 steel ball under dry friction condition. It is seen that the coating prepared without NaF has a higher coefficient of friction than the coating prepared with NaF. The mean friction coefficient of the former is 0.19, while that of the latter is 0.16. In both cases, the friction coefficient increases with the extending of sliding distances, which should be owing to the nodules and cracks left on the surface of the coating (shown in Fig. 2). When the steel ball wears against the coated samples, those nodules and cracks would be ground off the surface and wear debris have the ploughing action in the friction surface. This causes the friction coefficient increasing with extending the sliding distances.

4. Discussion

During the MAO process, the substrate is firstly dissolved and loses metal brightness, but this process only lasts for a few seconds. Subsequently a thin transparent passive film forms on the anode surface. Accompanied by the aluminium oxide layer growing, the coating becomes more insulating, so the higher voltage is needed. The countless sparks moving rapidly on the surface of the sample can be observed when the anodic potential is increased up to several hundred volts. In fact, the lifetime of every spark or microarc is less than 10 μs, but the instantaneous temperature in the spark or the microarc zone is high enough to cause Al_2O_3 to melt and form complex compounds [6]. These compounds are composed of oxides coming from the substrate material and the electrolyte.

When fluoride is added into the aluminate solution, F^- would take part in the complex MAO processing, and has effects on the structure and properties of the formed ceramic coating. At the beginning of the MAO process, when the solution containing NaF, the cell voltage goes up faster and has a higher voltage, which is mainly induced by the electrolyte conductivity increasing with the addition of F^-. When sparks flashing all over the anode surface, the oxide film grows and becomes more insulating. During this period, electrochemical interaction of the electrolyte with the substrate metal through the insulating oxide layer on the surface is thermally stimulated. It results in the local growth and the propagation of the dielectric coating. As shown in Fig. 3a, there are microholes in the outer layer of the coating, and the diameter of these microholes is about 1 μm. As well, there are some shrinkage pipes in the inner compact layer [10]. Such structure provides a space to allow F^- ions entering into the coating and transferring forward to the anode under the function of the electric field force. The F^- ions lying in the middle of the coating not only provide a lower resistance path which causes the rate of voltage as a function of time decreased (shown in Fig. 1), but also attract the Al^{3+} ions coming into the coating by the charge force. When the microarc discharge occurs in a pore, the adjacent area of the coating with micropore structure is strongly heated. The Al^{3+} ions will have reaction with oxygen anions from water or hydroxyl to generate liquid Al_2O_3, which is then solidified to form α-Al_2O_3 and γ-Al_2O_3. The difference in the cooling rate of the molten alumina in the microarc zone results in the different contents of α-Al_2O_3 and γ-Al_2O_3 contents between the external and the internal layers of a coating. The higher

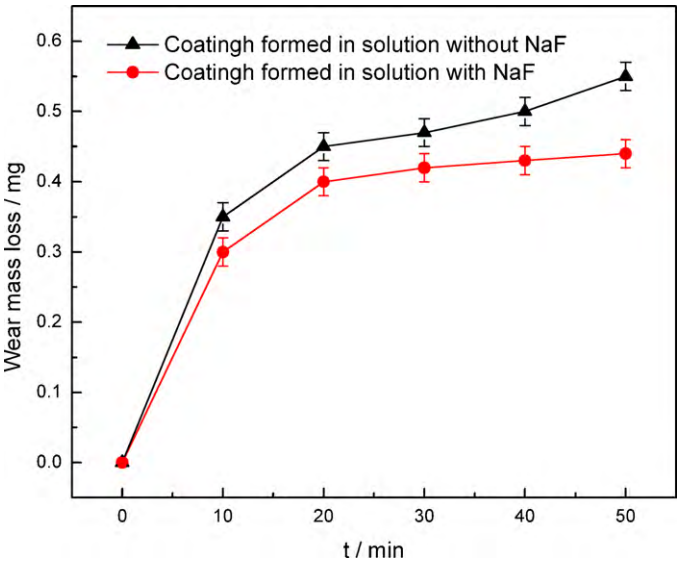

Fig. 8. Variation of wear mass loss of ceramic coatings with test duration.

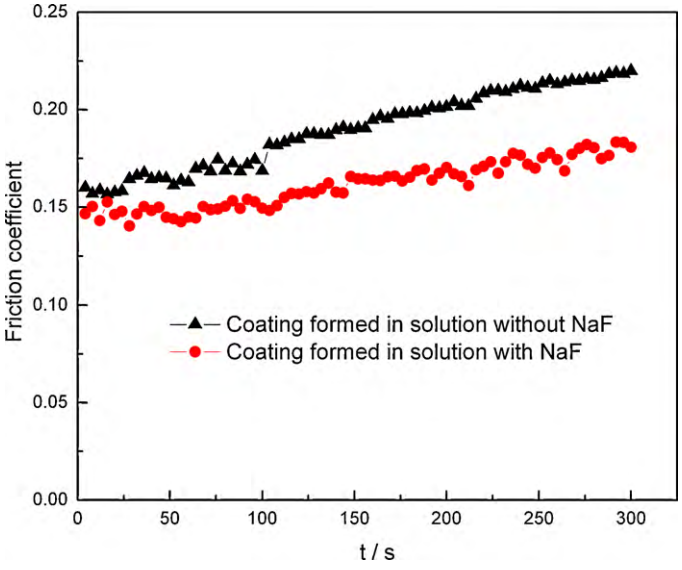

Fig. 9. Friction coefficient of ceramic coatings as a function of time.

cooling rate at the external layer favors the formation of γ-Al_2O_3 phase. On the contrary, α-Al_2O_3 phase is easily yielded in the internal layer with a lower cooling rate [9]. If there are more Al^{3+} ions in the micropores, these ions could reduce the porosity (shown in Fig. 2). This structure is beneficial to prevent the solution quenching on the melting alumina, which results in the inner layer having a lower cooling rate and getting a thicker layer (shown in Fig. 3). The Al^{3+} ions in the micropores deposit in the coating will cause the coating becoming thicker. However, according to Fig. 3, the coating formed in the solution containing NaF has the similar thick with the coating formed in the solution without NaF. This should be attributed to the higher negative voltage possessed by the solution with NaF. The ceramic coating is mainly formed during the anode process, while the cathode process actually hinders the increase of the thickness, for it leads to the dissolution of some oxide phases on the surface of the coating [25]. Therefore, both the coatings formed with and without NaF have similar thickness.

The ceramic coating formed by MAO process can sharply improve the corrosion resistance of the Al alloys. However, there are microholes and microcracks in the coating, which allows the penetration of corrosive liquids, leading to the chemical attack in the substrate. The coating formed with NaF has a thicker inner compact layer and less microhole left on the surface, so the general and the pitting corrosion resistances are both improved (shown in Fig. 5 and Fig. 6).

The hardness is sensitive to the presence of porosity. For example, 20% porosity is expected to reduce the hardness from the fully dense value near 60–70% [5,26]. The coating formed with NaF has a lower porosity than that formed without NaF. Lower porosity of the surface gives the coating better hardness. Just as shown in Fig. 7, the NaF added into the solution can improve the hardness of the coating.

Tribological characteristics are bound up with the structure of materials. When ceramic coatings worn against the GCr15 steel ball under high load, the external porous top layer of the coatings was worn off at the beginning, then the dense intermediate layer was revealed. Obviously, the coating bearing a thinner external loose layer and a thicker inner compact layer has a lower weight loss and a better abrasive resistance (shown in Fig. 8). The friction coefficient is influenced by the roughness of the initial friction surface [27]. The less rough surface of the coating formed with NaF can contribute to the lower friction coefficient at the beginning. With the sliding distance increasing, the nodules of the coating would be ground off the surface, and wear debris have the ploughing action in the friction surface. The surface of the coating formed without NaF has the features of island-like structure and lower hardness, which will result in more wear debris entering into the friction surface, thus causing a higher friction coefficient (shown in Fig. 9).

5. Conclusion

The microstructure and properties of the ceramic coating formed in electrolyte solution with and without NaF by the MAO process have been investigated. All the coated specimens have a double-layer structure and a rough porous surface. The F^- ions can permeate into the coating under electric field force, thus inducing the distribution of Al^{3+} ions among the microholes lying in the coating, which leads to greatly decreasing the surface roughness and increasing the thickness of the inner compact layer. This structure results in both corrosion resistance and tribological properties of the ceramic coating greatly improved.

Acknowledgement

This work was financially supported by Natural Science Foundation of Heilongjiang Province of China (Grant No. E2007-36).

References

[1] S.P. Chakraborty, S. Banerjee, I.G. Sharma, B. Paul, A.K. Suri, J. Alloys Compd. 477 (2009) 256–261.
[2] H. Allachi, F. Chaouket, K. Draoui, J. Alloys Compd. 475 (2009) 300–303.
[3] L.O. Snizhko, A.L. Yerokhin, A. Pilkington, N.L. Gurevina, D.O. Misnyankin, A. Leyland, A. Matthews, Electrochim. Acta 49 (2004) 2085–2095.
[4] L.R. Krishna, K.R.C. Somaraju, G. Sundararajan, Surf. Coat. Technol. 163 (2003) 484–490.
[5] J.A. Curran, T.W. Clyne, Acta Mater. 54 (2006) 1985–1993.
[6] A.L. Yerokhin, X. Nie, A. Leyland, A. Matthews, S.J. Dowey, Surf. Coat. Technol. 122 (1999) 73–93.
[7] A.A. Voevodin, A.L. Yerokhin, V.V. Lyubimov, M.S. Donley, J.S. Zabinski, Surf. Coat. Technol. 86 (1996) 516–521.
[8] P.A. Dearnley, J. Gummersbach, H. Weiss, A.A. Ogwu, T.J. Davies, Wear 229 (1999) 127–134.
[9] W.B. Xue, Z.W. Deng, R.Y. Chen, T.H. Zhang, Thin Solid Films 372 (2000) 114–117.
[10] J.A. Curran, T.W. Clyne, Surf. Coat. Technol. 199 (2005) 168–176.
[11] P. Su, X.H. Wu, Y. Guo, Z. Jiang, J. Alloys Compd. 475 (2009) 773–777.
[12] M. Uchikoshi, K. Imai, K. Mimura, M. Isshiki, J. Mater. Sci. 43 (2008) 5430–5435.
[13] Z.P. Yao, Z.H. Jiang, F.P. Wang, W. Xue, Appl. Surf. Sci. 253 (2007) 4267–4272.
[14] W.B. Xue, X.L. Shi, M. Hua, Y.L. Li, Appl. Surf. Sci. 253 (2007) 6118–6124.
[15] B. Lonyuk, I. Apachitei, J. Duszczyk, Surf. Coat. Technol. 201 (2007) 8688–8694.
[16] L.R. Krishna, A.S. Purnima, N.P. Wasekar, G. Sundararajan, Metall. Mater. Trans. A 38A (2007) 370–378.
[17] J. He, Q.Z. Cai, H.H. Luo, L. Yu, B.K. Wei, J. Alloys Compd. 471 (2009) 395–399.
[18] G.H. Lv, W.C. Gu, H.A. Chen, W.R. Feng, M.L. Khosa, L. Li, E.W. Niu, G.L. Zhang, S.Z. Yang, Appl. Surf. Sci. 253 (2006) 2947–2952.
[19] Z.P. Yao, Z.H. Jiang, X.L. Zhang, J. Am. Ceram. Soc. 89 (2006) 2929–2932.
[20] Y.K. Wang, L. Sheng, R.Z. Xiong, B.S. Li, Surf. Eng. 15 (1999) 109–111.
[21] H.Y. Zheng, Y.K. Wang, B.S. Li, G.R. Han, Mater. Lett. 59 (2005) 139–142.
[22] P.I. Butyagin, Y.V. Khokhryakov, A.I. Mamaev, Mater. Lett. 57 (2003) 1748–1751.
[23] X. Nie, E.I. Meletis, J.C. Jiang, A. Leyland, A.L. Yerokhin, A. Matthews, Surf. Coat. Technol. 149 (2002) 245–251.
[24] C.N. Cao, X.W. Yu, Corros. Sci. Prot. Technol. 13 (2001) 49–51.
[25] A.L. Yerokhin, X. Nie, A. Leyland, A. Matthews, Surf. Coat. Technol. 130 (2000) 195–206.
[26] I.J. McColm, Ceramic Hardness, NY: Plenum Press, New York, 1990.
[27] N.P. Suh, N. Saka, Fundamentals of Tribology, The MIT Press, Cambridge, 1978.